

Quantifying the kinetic parameters of prion replication

Joanna Masel^{a,*}, Vincent A.A. Jansen^a, Martin A. Nowak^b

^a*Wellcome Trust Centre for the Epidemiology of Infectious Disease, Department of Zoology, University of Oxford,
South Parks Road, Oxford OX1 3PS, UK*

^b*Institute for Advanced Study, Olden Lane, Princeton, NJ 88540, USA*

Received 9 December 1998; received in revised form 4 February 1999; accepted 4 February 1999

Abstract

The mechanism of protein-only prion replication is controversial. A detailed mathematical model of prion replication by nucleated polymerisation is developed, and its parameters are estimated from published data. PrP-res decay is around two orders of magnitude slower than PrP-sen decay, a plausible ratio of two parameters estimated from very different experiments. By varying the polymer breakage rate, we reveal that systems of short polymers grow the fastest. Drugs which break polymers could therefore accelerate disease progression. Growth in PrP-res seems slower than growth in infectious titre. This can be explained either by a novel hypothesis concerning inoculum clearance from a newly infected brain, or by the faster growth of compartments containing smaller polymers. The existence of compartments can also explain why prion growth sometimes reaches a plateau. Published kinetic data are all compatible with our mathematical model, so the nucleated polymerisation hypothesis cannot be ruled out on dynamic grounds. © 1999 Elsevier Science B.V. All rights reserved.

Keywords: Prion diseases; Replication mechanism; Nucleated polymerisation; Mathematical model

1. Introduction

Transmissible spongiform encephalopathies (TSEs) are fatal neurodegenerative diseases. TSEs are found in a variety of mammals, including scrapie in sheep, bovine spongiform encephalopathy in cattle, and kuru and Creutzfeldt–Jakob disease (CJD) in humans. The nature of the infectious agent in TSEs has long been controversial, since its properties are unlike those of any

previously known virus or viroid. It was proposed that the infectious agent, known as a prion, consists solely of a proteinaceous particle [1,2]. This was identified as a form of the PrP protein [1]. According to this hypothesis, an infectious proteinase K-resistant form of PrP (PrP-res or PrP^{Sc}) converts the normal proteinase K-sensitive form of PrP (PrP-sen or PrP^C) into PrP-res. The protein-only hypothesis has not been directly proved, but an abundance of circumstantial evidence has won it widespread support. There are many recent reviews critically examining the evidence [3–6].

Self-replication of a protein agent is a novel

* Corresponding author. Fax: +44-18654-310447; email: joanna@volterra.zoo.ox.ac.uk

concept. The mechanism is not immediately clear, and several mechanisms have been proposed. In the heterodimer mechanism [7] (Fig. 1a), a single PrP-res molecule catalyses the conformational change of a single PrP-sen molecule into PrP-res. According to co-operative autocatalysis [8,9] (Fig. 1b), a mixed aggregate of PrP-res and PrP-sen converts to an aggregate of PrP-res via allosteric interactions. According to nucleated polymerisation [8,10,11] (Fig. 1c), PrP-res is a polymeric form of PrP, while PrP-sen is monomeric. Polymerisation is very slow below a critical size. Above this size, the polymer is stabilised, and further polymerisation is comparatively rapid. The slow nucleation process can be circumvented by adding an infectious ‘seed’.

Prion diseases have some unusual kinetic features. Spontaneous disease is rare, but disease progresses inevitably after infection. Disease is

characterised by an extremely long and precisely reproducible incubation period, followed by a brief and invariably fatal clinical disease. The length of the incubation period is dependent on the inoculum dosage, the prion strain, and the level of PrP expression in the animal.

Kinetic modelling is a tool which uses these unusual kinetic features to help determine whether a proposed mechanism is plausible. Any proposed mechanism will contain a number of assumptions. Formulating a mechanism as a mathematical model makes these assumptions more transparent. The model can then be critically examined for internal consistency and consistency with available data. To do this, it is helpful to determine the values of parameters specified in the model. For many purposes, it is enough to estimate a parameter to within an order of magnitude. If a model creates no direct

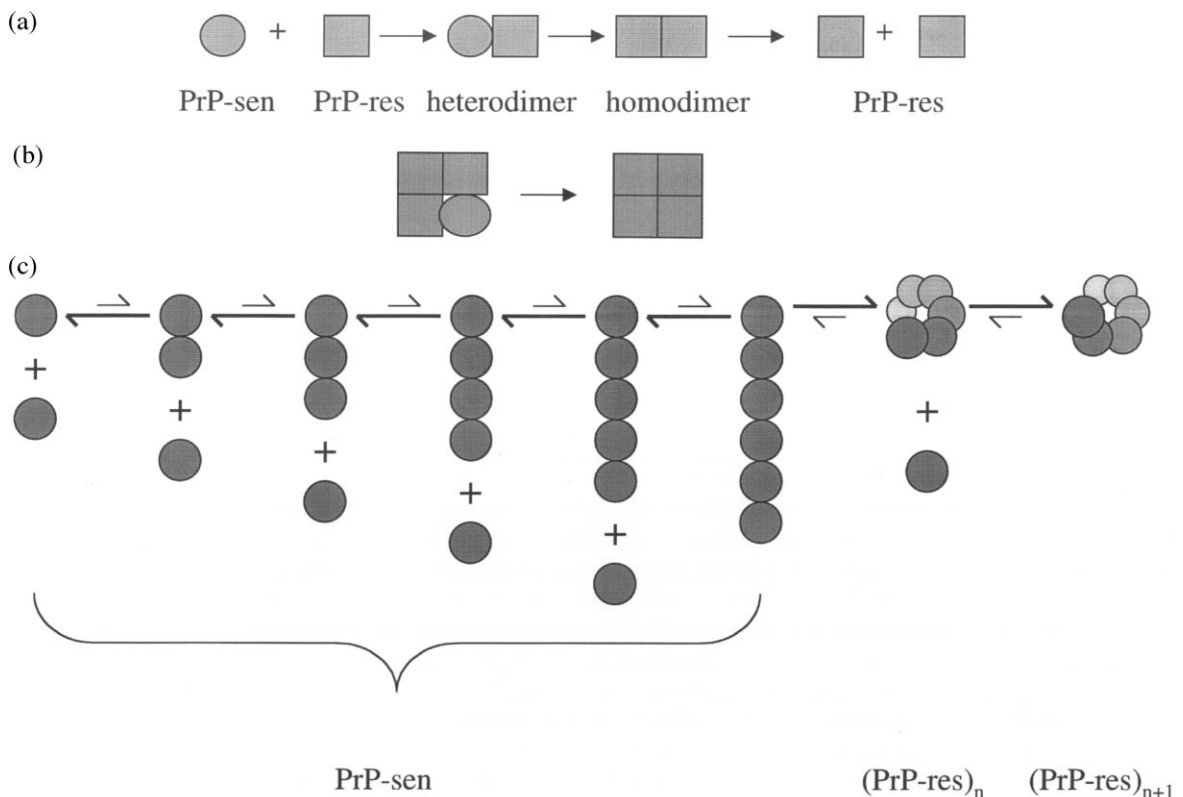


Fig. 1. Proposed mechanisms of prion replication. (a) Heterodimer mechanism [7]. (b) Co-operative autocatalysis [8,9]. (c) Nucleated polymerisation mechanism [10,11] with minimum nucleation size $n = 6$.

contradictions and the calculated parameter values seem realistic, then the assumptions are reasonable and the model is plausible. If not, then a new model or mechanism should be considered. If a simple model fits the data, then a large number of modified, more complex models will fit the same data, and there is no way to choose between the many complex models. For this reason, if a simple model fits the data as well as a more complex model, then we use the simpler model.

Some hypothesised mechanisms include molecules other than the PrP protein, such as a virino [12] or protein X [13]. Here we examine the simplest possible models first, these being models without cofactors. If the simpler models are sufficient, this does not prove that no cofactors are present, since cofactors which are present in excess will not be apparent in kinetic data. It does show them to be unimportant for the dynamics of the system. If simpler models prove kinetically insufficient, we will then consider the kinetic contribution of cofactors.

A consistent model must explain why spontaneous prion disease is so rare, whereas disease progresses inevitably after inoculation. A single infectious particle will spread and cause disease unless it is rapidly degraded, so spontaneous prion production must be significantly slower than prion degradation. When this is considered in calculating the parameters of a heterodimer model, only an implausible parameter range is possible [8].

This makes the heterodimer mechanism seem highly unlikely.

Co-operative autocatalysis and nucleated polymerisation do not suffer from this difficulty [8]. These two mechanisms are also supported by the failure to dissociate infectivity from aggregated forms of PrP. The rich diversity of prion strains is also harder to explain by the multiple, non-inter-converting conformations of a single protein chain than it is by a mechanism involving the geometric interactions between protein subunits.

Scrapie-associated fibrils or ‘prion rods’ localise with disease-specific PrP and may well be the pathogenic form of PrP. They appear as unbranched linear polymers when observed using electron microscopy [14]. For this reason, we assume that polymers are linear on a macroscopic level, although they may be helical on a microscopic level.

The nucleated polymerisation mechanism has two slight advantages over the co-operative autocatalysis mechanism, although there is no hard evidence to distinguish the two. Firstly, co-operative behaviour is usually associated with globular rather than linear aggregates, and pathogenic PrP appear to be linear. Secondly, nucleated polymerisation is much simpler.

The advantages and disadvantages of the three mechanisms are summarised in Table 1. Nucleated polymerisation seems the most likely candidate, and worthy of further development and testing. In this paper we develop and extend a formal model of nucleated polymerisation pro-

Table 1
Comparison of the three replication mechanisms

	Heterodimer	Co-operative autocatalysis ^a	Nucleated polymerisation
Explains kinetics of spontaneous generation	×	✓	✓
Explains the association between infectivity and aggregated PrP	×	✓	✓
Explains strain diversity	×	✓	✓
Explains linear appearance of the fibrils	×	×	✓
Relatively mathematically tractable	✓	×	✓

^aLinear fibrils with diameters wider than a single molecule may occur in some co-operative models. In the limiting case when the fibril diameter is constant and aggregation is the rate-limiting step, this is mathematically equivalent to our treatment of nucleated polymerisation.

posed by Nowak et al. [15]. We use published data on the unusual kinetic features of prion diseases to quantify the parameters.

2. Nucleated polymerisation model

Formal models of linear nucleated polymerisation have been developed for other biological systems [16–18]. Our prion model, illustrated in Fig. 2, is more explicit in incorporating terms λ for production, d and a for degradation and b for polymer breakage. Polymer extension is treated as a one-way process with rate β . Nucleation is considered negligibly slow. The terms x , y and z count PrP-sen, PrP-res polymers and total PrP-res.

More formally, let x be the abundance of PrP-sen monomers and let y_i be the abundance of PrP-res polymers containing i subunits. The total abundance of PrP-res polymers summed over all sizes is $y = \sum y_i$. The total abundance of PrP-res subunits is $z = \sum iy_i$. PrP-sen is produced at the constant rate λ , and is metabolically degraded at rate d . β_i gives the polymerisation rate of a polymer of i subunits, i.e. monomers are added

onto PrP-res polymers of length i at the rate $\beta_i xy_i$. For a linear polymer, it is reasonable to assume that β_i is a constant β .

PrP-res polymers are degraded at rate $a \ll d$. Small polymers are degraded at the same rate as large polymers, which is realistic for degradation mechanisms such as incorporation into plaques or engulfment by macrophages.

A polymer of size i breaks into two pieces of size j and $i-j$ at rate $b_{i,j}$. Assume that $b_{i,j}$ is a constant b for $i \geq n$. In a nucleated polymerisation mechanism, polymers below a critical size n are unstable and disintegrate rapidly into PrP-sen monomers. In the model by Nowak et al., this occurs rapidly at rate u [15]. In this model we make an additional approximation, namely that $b_{i,j}$ is infinite for $i < n$. This approximation is valid if u can be considered instantaneous or if nucleation kinetics put $y_{i < n}$ at a low but steady state. The additional approximation greatly simplifies the mathematics.

This system is analysed in detail in Appendix A, and can be described by three coupled differential equations:

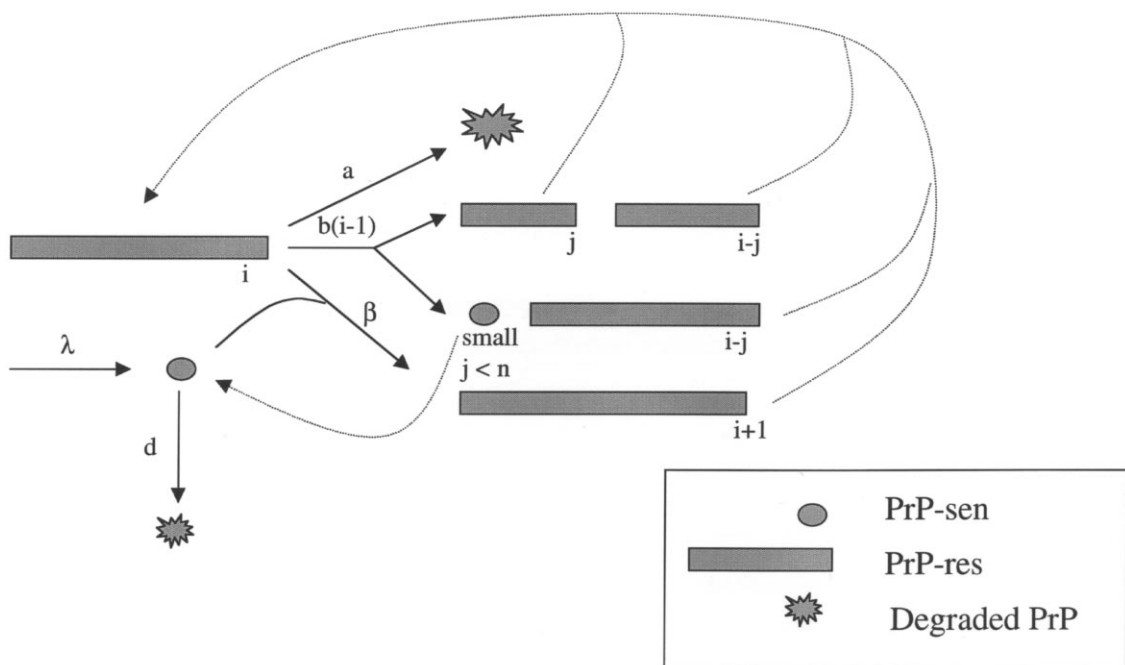


Fig. 2. Detailed kinetic model of nucleated polymerisation.

$$\begin{aligned} \frac{dx}{dt} &= \lambda - dx - \beta xy + n(n-1)by \\ \frac{dy}{dt} &= -ay + bz - (2n-1)by \\ \frac{dz}{dt} &= \beta xy - az - n(n-1)by \end{aligned} \tag{1}$$

In the absence of infection, PrP-sen is at the equilibrium $X_0 = \lambda/d$, and remains at this level for some time after infection. The average size $s = z/y$ of the polymers quickly converges to the equilibrium

$$\bar{s} \approx n - \frac{1}{2} + \sqrt{\frac{\beta X_0}{b}} \tag{2}$$

The distribution of sizes also reaches an equilibrium, and an example is shown in Fig. 3.

After the average size reaches equilibrium, y and z accumulate exponentially. The exponential growth rate r is given by

$$r = b(\bar{s} - 2n + 1) - a \tag{3}$$

until x begins to decline. It is worth noting that without the breakage term b , the average size s does not reach a steady state and growth is not exponential.

The basic reproductive ratio R_0 is defined as the average number of infectious particles that one infectious particle will give rise to before being destroyed [19]. Infection will spread if $R_0 > 1$. Here, the average lifetime is the inverse of the death rate, so the basic reproductive ratio is given by the birth rate divided by the death rate. During each breakage, consider the left fragment the parent and the right fragment the offspring. Death can occur either by degradation at rate a or by breakage such that the left fragment is too small to be viable, so the death rate is $a + b(n-1)$. The growth rate $r = \text{birth rate} - \text{death rate}$, so we derive

$$R_0 = \frac{b(\bar{s} - n)}{a + b(n-1)} \approx \frac{\sqrt{\beta X_0 b} - (b/2)}{a + b(n-1)} \tag{4}$$

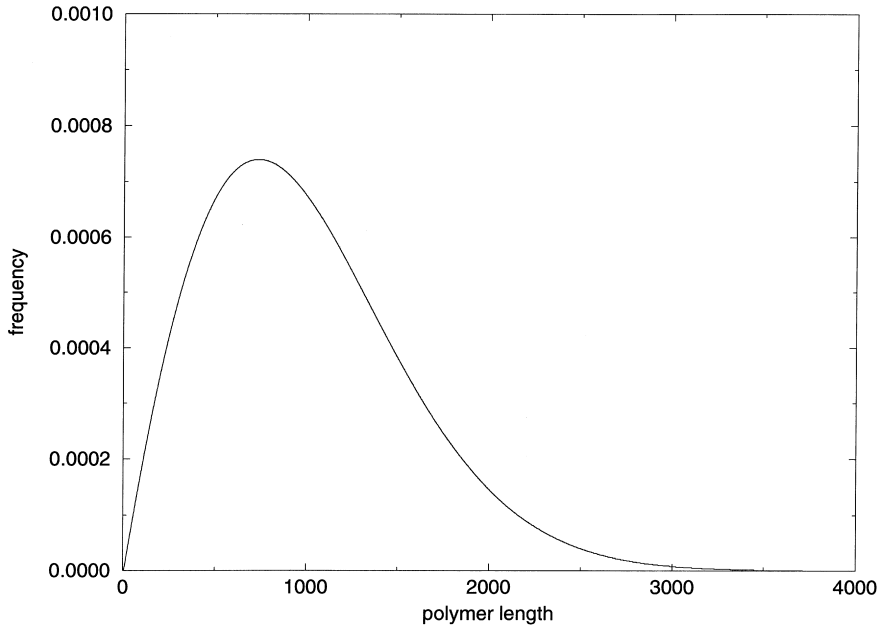


Fig. 3. The distribution of sizes shown here is calculated by letting $w_i = y_i/y$. Then for $i \geq n$, $dw_i/dt = bX_0(w_{i-1} - w_i) + b(s - 2n + i)w_i + 2b\sum_{j=i+1}^{\infty} w_j$. At equilibrium, we have $w_i = 0$ for $i < n$, and for $i \geq n$ we have the recursive definition $w_i = \frac{(\beta X_0/b)w_{i-1} + 2 - 2\sum_{j=i}^{\infty} w_j}{(\beta X_0/b) + \sqrt{(\beta X_0/b) + (1/4)} + i - n + (3/2)}$. w_i is determined by the quantity $\beta X_0/b$, which in turn is determined by \bar{s} and n . The size distribution is calculated numerically and plotted for $\bar{s} = 1000$, $n = 6$.

3. Quantifying kinetic parameters

The model is specified by six independent parameters, given as a , b , β , d , n and λ . The model can be rearranged as shown in Eq. (11) in Appendix A, and can be given in terms of six different independent parameters: r , R_0 , d , n , \bar{s} , and one of β , λ or X_0 . In Section 3 we quantify r , R_0 and d from published data and estimate n and \bar{s} . Unfortunately, this gives us only five parameters, so the model is under-specified by current data. Nevertheless, r and R_0 can be rearranged to give a , and this can be compared to d to see whether it fits the predicted relationship $a \ll d$.

3.1. Measuring the growth rate r

The exponential growth rate r can be measured in three ways (Table 2). Firstly, growth in the number of infectious units can be traced, which should correspond to growth in y . Secondly,

growth in PrP-res accumulation can be measured, which should correspond to growth in z . Thirdly, the standard curve used to measure infectivity by the incubation time assay [20] gives an indirect measure of growth in y .

In Method 1, brain homogenates are assayed for infectivity at various time points after inoculation. The number of infectious units is plotted on a log scale against time, and a growth curve is obtained. Our model predicts exponential growth, which should be seen as a straight line. Modelling exponential growth works well, and growth rates estimated from the linear portions of the curves are given in Table 2. The latest time points sometimes approach a plateau, which can be explained either as an approach towards equilibrium in our model, or by another mechanism described in Section 4.2.

Method 2 measures the growth of the PrP-res protein, which is more difficult. PrP-res levels are below the detection limit of most assays for a large portion of disease progression, leading some

Table 2
Exponential growth rate r (day⁻¹)

	Infectivity accumulation estimate of r	PrP-res accumulation estimate of r	Incubation time assay estimate of r	Best guess
Chandler mouse scrapie			0.214, 0.235, 0.177 [21], 0.140 [22], mean: 0.192	0.17
139A mouse scrapie			0.0576 [23] (small inocula)	0.05
263K hamster scrapie	0.182 [24], 0.267 [25], 0.248 [26], 0.154 [27], mean: 0.213	0.152 [26]		0.17
Sc237 hamster scrapie	0.142 ^a [28], 0.137 [29], mean: 0.140	0.108 [28]	0.328 [30] (large inocula) 0.121 [30] (small inocula)	0.11
Fukuoka-1 hamster CJD	0.0375 [31], 0.0760 [32], mean: 0.0568 ^b		0.109 [32]	0.05
Mouse CJD			0.078 [34]	0.07

^a In the original paper, linear regression over all data points gave $r = 0.120$. Our estimate was derived from the linear portion of the published graph.

^b The data points are very scattered in both these studies. We ignored measurements less than 6 h after inoculation, and pooled measurements taken before and after heating brain homogenates. We used regression weighted against the standard error of each measurement.

investigators to conclude that significant protein accumulation occurs suddenly and only in the late stages of the infection. Exponential growth may still be occurring below the detection limit of these assays. Two studies used more sensitive assays for PrP. One study purified PrP-res by sedimentation [26] and the other digested brain homogenates with proteinase K to eliminate other proteins [28]. These two studies detected exponential growth in PrP-res from quite early in the disease. The exponential curve fits well, confirming the model, but the growth rates are slower than those derived by Method 1. Two alternative explanations for this anomaly are given in Sections 4.1 and 5.1.

Method 3 takes advantage of the fact that incubation times depend on the inoculum dose and are precisely reproducible. A standard curve relates incubation times to the log dilution of the inoculum. All or part of the curve is often highly linear. This linear section implies an exponential

growth in the number of infectious units, derived from the time it takes for a smaller inoculum to ‘catch up’ with a large inoculum. The curve is not entirely linear [20,30,35,36], an anomaly which is explained in Section 4.1.

In summary, there is good evidence for slow exponential growth throughout most of the incubation period. In the final column of Table 2, we give an estimate of r for each prion strain, taking into account the clearance phenomena discussed in Section 4.2 and the circumstances of the individual studies.

3.2. Measuring the basic reproductive ratio R_0

Studies of transgenic and knockout mice have shown that incubation time is inversely related to the level of PrP expression [21,31,37–40]. Here we use the precise quantitative relationship between the two to measure the basic reproductive ratio R_0 . This can be done by three slightly

Table 3
Basic reproductive ratio R_0

Mouse prion strain	PrP ^{+/+} incubation (days)	PrP ^{+/-} incubation (days)	Criteria for incubation time ^a	u	R_0	Best guess R_0	Ref.
ME7 scrapie	50	100	PrP labelling	0.50	2.4	3	[37]
	75–100	150	PrP labelling	0.50–0.67	2.4–8.2		
	100	150	Vacuolation	0.67	8.2		
	130	220	First symptoms	0.59	3.5		
	160	280	Terminal stage disease	0.57	3.2		
Chandler scrapie	158	290	Illness ^b	0.55	2.8	2	[21,38]
	171	415					
	156	426	Illness ^b	0.37	1.9		
	169	430	Death	0.39	1.9		
Fukuoka-1 CJD	138	259	Illness	0.53	2.7	3	[31]
	143	269	Death	0.53	2.7		
	$r = 0.0219 \text{ days}^{-1}$	$r = 0.0375 \text{ days}^{-1}$	N/A	0.58	3.3		
Sc237 scrapie	Transgenic mouse studies		Illness		1.5	1–2	[39]

^aTiming illness is more subjective than timing death, but less likely to involve a plateau phase. The patterns and intensities of PrP labelling and vacuolation give even earlier, but still less precise time points.

^bThese studies used the same mice and the same scrapie strain, but noted very different incubation times. Different criteria were used for assessing the onset of symptoms.

different methods, and the results are shown in Table 3.

For the first method, let u be the ratio of the incubation times in two strains of mice, and let v be the ratio of PrP expression levels. In Appendix A, we assume that exponential growth continues without a plateau phase and show that

$$R_0 \approx \frac{1-u}{(1/\sqrt{v})-u} \quad (5)$$

Incubation times in heterozygous PrP^(+/-) knockout mice were compared to wild-type littermates to estimate the R_0 (Table 3). Heterozygotes appear to have half the wildtype level of PrP [37,38], so $v = 2$.

In the second method, the growth rates of CJD infectivity in hamster brains are measured directly in wild-type and PrP^(+/-) mice [31], as described in Section 3.1. Eq. (5) is used, but this time u is the inverse ratio of the growth rates.

The third method fits a curve when more than two strains of mice are available. The relationship between PrP-sen levels and the incubation time of scrapie strain Sc237 in transgenic mice expressing hamster PrP [39] gives $R_0 = 1.5$ as shown in Fig. 4.

All the methods give similar R_0 figures, supporting our methods. In the last column of Table 3, we have put a consensus estimate for R_0 for each prion strain.

3.3. Measuring the PrP-sen degradation rate d

PrP-sen turnover has been studied in mouse neuroblastoma cells by pulse-chase [41,42]. In this system, PrP-sen has a half-life of 3–6 h, making $d \approx 3\text{--}5 \text{ day}^{-1}$.

3.4. Estimating the minimum nucleation size n

Can we derive the minimum nucleation size n

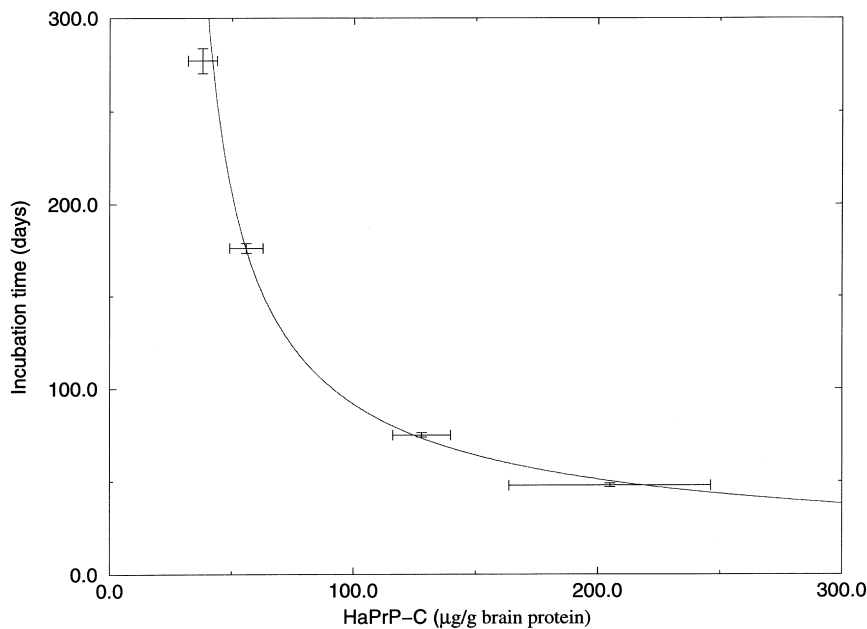


Fig. 4. The model predicts a relationship between the PrP level X and the scrapie incubation time t described by the equation $\sqrt{X} = A + (B/t)$ where $A = (\sqrt{X_0}/R_0)$ and B is some constant. This equation is fitted to data from four lines of transgenic mice expressing hamster PrP and infected with scrapie strain Sc237 [39]. Using non-linear least-square regression, weighting according to the inverse of the standard errors of both expression levels and incubation times, we get $A = 4.7$ and $B = 483$. This fit is shown in the figure, and is the best of many plausible fits. The data also fits the simpler equation $X = B/t$. At $52 \mu\text{g g}^{-1}$ brain protein, the level of expression in a wild-type hamster, $R_0 = 1.5$.

from structural considerations? The structure of PrP-sen is known from NMR [43–45], but far less is known about the structure of PrP-res polymer, which is some form of fibrillar amyloid.

If the polymer were a helix, this would give a structural explanation for the minimum nucleation size. In a helical model, a linear polymer of size n would fold back on itself, form multiple stabilising bonds, and become a seed. It seems unlikely that $n < 3$ or $n > 30$. Spheres of four to six PrP molecules can be broken off large PrP-res polymers by sonication. The spheres are not infectious, are sensitive to proteinase K and have an alpha-helical content comparable to PrP-sen [46]. This provides circumstantial evidence that $n > 6$. A more definite determination of n should eventually be possible. This measurement could come from the kinetics of nucleation, since the rate of nucleus formation should be proportional to monomer concentration to the power $n - 1$ [47]. A solved structure of the PrP polymer and/or sedimentation and filtration studies could also help determine the value of n .

3.5. Estimating the mean polymer length \bar{s}

The ratio of PrP-res molecules to one LD₅₀ unit has been estimated as 10^4 – 10^5 [48], 10^4 [49], 10^5 [1,50] and $\geq 10^5$ [5]. It is very difficult to estimate this ratio, since there is often an imperfect correlation between titre and protein concentration. In a study of purified fractions, the ratio fell from 4×10^6 21 days after inoculation to 3×10^5 at day 77 [26].

Assuming a 10^5 :1 ratio of PrP-res molecules to LD₅₀ units and clearance (see Section 4.1) leading to a 100:1 ratio of infectious particles to LD₅₀ units gives $\bar{s} = 1000$. This figure may be very inaccurate and the range $\bar{s} = 100$ – $10\,000$ should be considered. This is compatible with the electron microscopy studies, where scrapie-associated fibrils appear to be approximately 14–16 nm wide, and 60–1500 nm long [14,51,52].

4. Extensions to the model

4.1. Clearance phenomena

When brain infectivity is assayed a few days

after intracerebral inoculation, the majority of the infectious agent can no longer be found. The rate of this clearance is highly variable (Table 4). This variability can explain anomalies arising from growth rate measurements.

The factors influencing the extent of inoculum clearance have not been definitively determined, but the size and strain of the inoculum and the exact protocol of inoculation may be important. The organ of origin [53] and chemical treatment [23] of inocula can alter infectivity estimates. To explain the two anomalies noted in Section 3.1, we propose that there is a non-specific response to intracerebral inoculation which varies with the level of antigenic stimulation. When more brain matter is injected, a greater proportion of infectivity is cleared. Most studies in Table 4 used large inocula containing a significant proportion of a homogenised brain, while one study used a smaller, more dilute inoculum. In support of our antigenic clearance hypothesis, this one study showed a significantly lower rate of clearance than the others.

The first anomaly is that the growth of PrP-res, representing z , is slightly slower than the growth of infectivity, representing y (Table 2). In other words, the mean size appears to fall during disease progression. This is counter-intuitive, since large amyloid plaques containing long fibres appear late in the disease.

The discrepancy in the growth rates can be explained by our antigenic clearance hypothesis. Early in infection, there is a low ratio of infectious particles to other brain material, and exten-

Table 4
Clearance of intracerebral inocula

Initial inoculum (log LD ₅₀ units)	Drop (log LD ₅₀ units)	Time (days)	Drop adjusted for growth over time	Ref.
6	1.5	5	1.7	[33]
7	> 4.8	4	> 5.1	[21]
7	1.8	7	2.3	[25]
6	7	1	7.1	[26]
7	2.5	0	2.5	[28]
	3.5	2	3.7	
3.9	0.3	7	0.8	[24]

sive clearance leads to underestimation of infectious titre. Later in infection, this ratio rises, and measured infectivity rises more than the actual rise in y .

The antigenic clearance hypothesis can also explain the second anomaly, the slight non-linearity of the incubation time standard curve. Here, smaller inocula are more dilute, and contain less contaminating brain material, so we expect less clearance with smaller inocula. Assume that if it were not for clearance phenomena, the curve would be linear. If the amount of inoculum lost in log units were directly proportional to the size of the inoculum, then the size differences between large inocula would be exaggerated, and a linear plot showing a faster rate of growth would be produced. If the inoculum lost in log units increases more than proportionally with the size of the inoculum, then the graph would no longer be linear. All growth estimates taken from incubation time assay curves would be overstated, but overestimation would be more pronounced with large inocula and minimised with small inocula. Unfortunately, small inocula lead to more scattered measurements on an incubation time assay. Measuring r using the incubation time assay can be highly inaccurate.

In summary, discrepancies between the theoretical model and data on growth rates can be explained by an antigenic clearance hypothesis.

4.2. Effect of compartments

Our model assumes that all sites of prion replication have the same levels of PrP-sen X_0 and of breakage b . Assume instead that these parameters vary between compartments, leading to variation in the growth rate. Also assume that cells in a compartment die after the accumulation of a critical level of PrP-res. PrP is no longer produced in this compartment, but existing PrP-res persists, perhaps in extracellular plaques. In agreement with this model, PrP-sen levels vary between regions of the uninfected brain [54], and specific neuronal subpopulations die early in infection [55].

In simulations of this compartmental model

(data not shown), the accumulation of PrP is very close to exponential for some time, until it is offset by the deaths of the most rapid PrP-res producing cells, and a plateau appears. This effect, rather than an approach to the equilibrium solution of Eq. (1), may explain the observed prion growth plateau often seen in animals.

4.3. Spatial effects

Our model does not include spatial effects. Infectivity may take some time to travel from the peripheral tissues to the brain. For example, infectivity takes a minimum of 14 days to reach the mouse brain via the optic nerve [56]. This should not affect the data used in this paper, since most follows from intracerebral inoculation. The spread of infectivity to the central nervous system following peripheral infection routes has been modelled elsewhere [57]. A similar course of exponential growth and disease progression occurs once prion infectivity has reached the central nervous system, irrespective of how it got there [27].

Diffusion within the brain occurs by at least two routes: axonal transport and diffusion through the extracellular space [35]. In this paper, we assume this diffusion is not a significant kinetic bottleneck. In support of this, both sides of the brain contain equal titres 5 days after intracerebral inoculation [33].

5. Discussion

5.1. Impact of the breakage parameter b

In our model, we assume that all polymers are subjected to the same breaking forces and that a polymer is equally likely to break at any position along its length. The cause of the breakage is not specified, but knowing the cause could help justify this assumption.

Shearing forces could well be significant, but these are dependent on the environment in which prion replication occurs. It is not yet known whether prion replication occurs in the extracellular space, at the plasma membrane or within a membrane compartment. Infection can be propa-

gated even when PrP expression is restricted to astrocytes [58], so intracellular neuronal replication is not essential.

An alternative cause of polymer breakage has come out of work on yeast prions. The chaperone Hsp104p is required for [PSI⁺] prion propagation in vivo, but overexpression of the chaperone eliminates the prion [59]. This strange phenomenon would be explained if Hsp104p broke yeast prions into smaller pieces [60,61]. Some as yet unidentified mammalian chaperone could perform the same task for PrP. Indeed, conversion of mammalian prions is promoted by intermediate levels of the chemical chaperone DMSO [62].

Rearranging Eqs. (2) and (3), we can express the dependence of the growth rate r on the breakage rate b according to

$$r \approx \sqrt{\beta X_0 b} - b(n - 0.5) - a \quad (6)$$

When everything except breakage is kept constant, growth is maximal when $\sqrt{(\beta X_0)/b} = 2n - 1$. This is equivalent to the condition $\bar{s} = 3n - 1.5$. So maximum growth is achieved with pools of quite small polymers, while the growth of pools of long polymers can be slow.

Chaperones causing the breakage may well be more active in some parts of the brain than in others. The large polymers seen by electron microscopy, and showing up in brain homogenates as PrP-res, may come from compartments with low levels of chaperone. Disease progression may be determined by some other replication site where replication occurs more quickly. Rapidly growing polymers may be too small to be seen.

Eq. (6) can explain why infectivity seems to accumulate faster than PrP-res. Compartments of small polymers may grow faster than compartments of large polymers, causing the overall mean size to fall over time.

Analysis of the breakage rate can have practical implications. For example, a drug which cures prions in vitro could act by increasing the breakage rate. If the effective dosage is lower in vivo, such a drug could well accelerate disease progression.

5.2. Comparing the parameters a and d

In Appendix A, we show that

$$a \approx \frac{r}{R_0 - 1} \quad (7)$$

In Table 5, we use this equation to calculate a from the measured quantities r and R_0 . Our estimate of a is highly sensitive to that of R_0 , which in turn is highly sensitive to the data, so our estimate of a is not very precise.

Nevertheless, $a \approx 0.02$ – 0.2 day⁻¹ seems reasonable as an order of magnitude calculation. Section 3.3 quantifies $d \approx 3$ – 5 day⁻¹. This estimate comes from a completely different experimental system to the ones used to quantify r and R_0 . This is a plausible comparison between a and d , and so quantifying parameters has led to reasonable results.

5.3. Other mechanisms

We can compare alternative mechanisms of prion replication using our mathematical framework. Some formulations of the heterodimer model allow for aggregation, but do not require it for the PrP-res state. This is equivalent to a special case of our model, derived by setting $n = 1$. This is a simpler model than ours, but has been shown to be kinetically implausible [8].

Other proposed mechanisms involve co-operative autocatalysis [8,9]. This is different to our model in two ways. Firstly, our model simplifies the conversion of PrP-sen to PrP-res to a single kinetic step. Autocatalytic models often contain two separate terms for aggregation and confor-

Table 5
Calculating the PrP-res degradation rate a

	r (day ⁻¹)	R_0	$a = r/(R_0 - 1)$ (day ⁻¹)
Chandler mouse scrapie	0.17	2	0.2
Sc237 hamster scrapie	0.11	1.5	0.2
Fukuoka-1 mouse CJD	0.05	3	0.03

mational conversion. Secondly, even if the two processes are combined into a single kinetic rate equation, β_i is not constant for $i \geq n$ in an autocatalytic model. Both of these modifications make the model mathematically more complicated and probably intractable. The kinetic model developed here has the advantage of simplicity.

Assuming constant β is plausible for a linear polymer but not for a globular aggregate. The support for this assumption rests on the linear appearance of scrapie-associated PrP as seen under electron microscopy.

5.4. Concluding remarks

A mechanism of protein self-replication may have wider implications. Although mice lacking PrP show no obvious phenotype, the rich diversity of prion strains suggests that PrP conversion and polymerisation is unlikely to be some freak accident not yet eliminated by natural selection. It is more likely that the pathogenic conversion process has a non-pathogenic counterpart serving some function in vivo. Modern biology is very heavily based on molecular genetic techniques, and the study of prions may provide a rare insight into post-translational molecular events. The prion analogues found in yeast may be useful in dissecting the mechanism, and much of the mathematical analysis presented here also applies to these systems.

Quantifying parameters for a formal model of nucleated polymerisation leads to consistent and realistic values. Nucleated polymerisation cannot be ruled out on kinetic grounds, and is a relatively simple and plausible mechanism worthy of further investigation. The formal model presented here provides a framework for explaining old experiments, and for designing new experiments to specifically test the mechanism.

Acknowledgements

We thank R. May, B. Caughey, D. Krakauer, R. Payne and R. Arnaout for stimulating discussions and critical reading of the manuscript. VAAJ gratefully acknowledges the support of The Well-

come Trust and Linacre College and JM of the Rhodes Trust.

Appendix A: Detailed nucleated polymerisation model

The definition of the model given in Section 2 gives the equations

$$\begin{aligned} \frac{dx}{dt} &= \lambda - dx - \beta xy + 2b \sum_{i=1}^{n-1} \sum_{j=i+1}^{\infty} iy_j \\ \frac{dy_i}{dt} &= \beta x(y_{i-1} - y_i) - ay_i - b(i-1)y_i \\ &\quad + 2b \sum_{j=i+1}^{\infty} y_j \quad \text{for } i \geq n \\ y_i &= 0 \quad \text{for } i < n \end{aligned} \quad (8)$$

This system can be closed by summation and described by three differential equations

$$\begin{aligned} \frac{dx}{dt} &= \lambda - dx - \beta xy + n(n-1)by \\ \frac{dy}{dt} &= -ay + bz - (2n-1)by \\ \frac{dz}{dt} &= \beta xy - az - n(n-1)by \end{aligned} \quad (1')$$

Similar summation is possible when the concentration of polymers below size n are in a steady state rather than zero.

While x is steady at $X_0 = \lambda/d$, the average size $s = z/y$ of the polymers quickly converges according to the differential equation

$$\frac{ds}{dt} = \beta X_0 - n(n-1)b + sb(2n-1-s) \quad (9)$$

until it reaches the equilibrium

$$\bar{s} = n - \frac{1}{2} + \sqrt{\frac{1}{4} + \frac{\beta X_0}{b}} \approx n - \frac{1}{2} + \sqrt{\frac{\beta X_0}{b}} \quad (2')$$

$\bar{s} \gg n$ so $\beta X_0 \gg b$, and the approximation is valid.

After the average size reaches equilibrium, ex-

ponential growth in the abundance of PrP-res over time t occurs according to

$$y(t) = y(0)e^{rt} \quad \text{and} \quad z(t) = z(0)e^{rt}$$

where $r = b(\bar{s} - 2n + 1) - a$

$$\approx \sqrt{\beta X_0 b} - nb - a + (b/2) \quad (3')$$

until x begins to decline.

Compare wild-type mice to mice with an altered level of PrP expression. Assume that λ is the only parameter that varies between strains, and let $v = \lambda_0/\lambda_1$ be the ratio of PrP expression between wild-type and mutant. Some criteria, such as the onset of the first symptoms, is used to recognise a time point in disease progression, and let $u = t_0/t_1$ be the ratio of the times taken to reach this point. Assume that exponential growth occurs at a constant rate from the time of inoculation. At some point a growth plateau may occur, but we assume that the plateau occurs after the measured point. Assume that the mice have the same levels of PrP-res in their brains at the given point. There is not a great deal of evidence available on this point, but most available evidence suggests that when mice develop symptoms, they have the same level of PrP-res in the brain, independently of their incubation period and level of PrP-sen expression [37–39] or route of inoculation [22]. One study contradicted this assumption [31], but here we accept the majority result and assume that sick mice have equal levels of PrP-res.

For two mice with different PrP expression levels,

$$y(0)e^{r_0 t_0} = y(t_0) = y(t_1) = y(0)e^{r_1 t_1},$$

giving

$$u = \frac{t_0}{t_1} = \frac{r_1}{r_0} \approx \frac{b\left[\sqrt{(\beta X_0)/(bv)} - n + (1/2)\right] - a}{b\left[\sqrt{(\beta X_0)/b} - n + (1/2)\right] - a} \quad (10)$$

From this we derive

$$\frac{1-u}{(1/\sqrt{v})-u} \approx \frac{\sqrt{\beta X_0 b}}{a+b(n-1/2)} \approx R_0 \quad (5')$$

Eqs. (2)–(4) give expressions for \bar{s} , r and R_0 . These can be rearranged to be expressed in terms of a , b and βX_0 .

$$b = \frac{r}{(\bar{s} - n)[1 - (1/R_0)]}$$

$$a = \frac{r}{R_0 - 1} \left(1 - \frac{R_0(n-1)}{(\bar{s} - n)} \right) \quad (11)$$

$$\beta X_0 = \frac{r(\bar{s} - n + 1)}{[1 - (1/R_0)]}$$

Since $\bar{s} \gg n$, we have

$$a \approx \frac{r}{R_0 - 1} \quad (7')$$

References

- [1] S.B. Prusiner, *Science* 252 (1991) 1515–1522.
- [2] J.S. Griffith, *Nature* 215 (1967) 1043–1044.
- [3] B. Chesebro, *Science* 279 (1998) 42–43.
- [4] B. Caughey, B. Chesebro, *Trends Cell Biol.* 7 (1997) 56–62.
- [5] A. Aguzzi, C. Weissmann, *Nature* 389 (1997) 795–798.
- [6] S.B. Prusiner, *Science* 278 (1997) 245–251.
- [7] F.E. Cohen, K.M. Pan, Z. Huang, M. Baldwin, R.J. Fletterick, S.B. Prusiner, *Science* 264 (1994) 530–531.
- [8] M. Eigen, *Biophys. Chem.* 63 (1996) A1–A18.
- [9] M. Laurent, *FEBS Lett.* 407 (1997) 1–6.
- [10] J.D. Harper, P.T. Lansbury, *Annu. Rev. Biochem.* 66 (1997) 385–407.
- [11] J.T. Jarrett, P.T. Lansbury, *Cell* 73 (1993) 1055–1058.
- [12] A.G. Dickinson, G.W. Outram, *CIBA Found. Symp.* 135 (1988) 63–83.
- [13] S.B. Prusiner, M.R. Scott, S.J. DeArmond, F.E. Cohen, *Cell* 93 (1998) 337–348.
- [14] M. Jeffrey, I.A. Goodbrand, C.M. Goodsir, *Micron* 26 (1995) 277–298.
- [15] M.A. Nowak, D.C. Krakauer, A. Klug, R.M. May, *Integr. Biol.* 1 (1998) 3–15.
- [16] F. Oosawa, M. Kasai, in: S.N. Timasheff, G.D. Fasman (Eds.), *Actin (Subunits in Biological Systems, Part A)*, Dekker, New York, 1971, pp. 261–330.
- [17] F. Oosawa, S. Asakura, *Thermodynamics of the Polymerization of Protein*, Academic Press, London, 1975.
- [18] S.N. Timasheff, in: C. Frieden, L.W. Nichol (Ed.), *The Self-Assembly of Long Rodlike Structures (Protein-Protein Interactions)*, Wiley, New York, 1981, pp. 315–336.

- [19] R.M. Anderson, R.M. May, *Infectious Diseases of Humans*, Oxford University Press, 1991.
- [20] S.B. Prusiner, S.P. Cochran, D.F. Groth, D.E. Downey, K.A. Bowman, H.M. Martinez, *Ann. Neurol.* 11 (1982) 353–358.
- [21] H. Bueler, A. Aguzzi, A. Sailer, et al., *Cell* 73 (1993) 1339–1347.
- [22] R.H. Kimberlin, C.A. Walker, *J. Comp. Pathol.* 88 (1978) 39–47.
- [23] R.A. Somerville, R.I. Carp, *J. Gen. Virol.* 64 (1983) 2045–2050.
- [24] R.H. Kimberlin, C.A. Walker, *J. Gen. Virol.* 67 (1986) 255–263.
- [25] M. Czub, H.R. Braig, H. Diringer, *J. Gen. Virol.* 69 (1988) 1753–1756.
- [26] D.C. Bolton, R.D. Rudelli, J.R. Currie, P.E. Bendheim, *J. Gen. Virol.* 72 (1991) 2905–2913.
- [27] D.C. Bolton, *J. Gen. Virol.* 79 (1998) 2557–2562.
- [28] K. Jendroska, F.P. Heinzel, M. Torchia, et al., *Neurology* 41 (1991) 1482–1490.
- [29] B. Oesch, D. Westaway, M. Walchli, et al., *Cell* 40 (1985) 735–746.
- [30] S.B. Prusiner, D.F. Groth, S.P. Cochran, F.R. Masiarz, M.P. McKinley, H.M. Martinez, *Biochemistry* 19 (1980) 4883–4891.
- [31] S. Sakaguchi, S. Katamine, K. Shigematsu, et al., *J. Virol.* 69 (1995) 7586–7592.
- [32] S. Sakaguchi, S. Katamine, K. Yamanouchi, et al., *J. Gen. Virol.* 74 (1993) 2117–2123.
- [33] L. Manuelidis, W. Fritch, *Virology* 216 (1996) 46–59.
- [34] L. Manuelidis, T. Sklaviadis, E.E. Manuelidis, *EMBO J.* 6 (1987) 341–347.
- [35] R. Hecker, A. Taraboulos, M. Scott, et al., *Genes Dev.* 6 (1992) 1213–1228.
- [36] D.A. Butler, M.R.D. Scott, J.M. Bockman, et al., *J. Virol.* 62 (1988) 1558–1564.
- [37] J.C. Manson, A.R. Clarke, P.A. McBride, I. McConnell, J. Hope, *Neurodegeneration* 3 (1994) 331–340.
- [38] H. Bueler, A. Raeber, A. Sailer, M. Fischer, A. Aguzzi, C. Weissmann, *Mol. Med.* 1 (1994) 19–30.
- [39] S.B. Prusiner, M. Scott, D. Foster, et al., *Cell* 63 (1990) 673–686.
- [40] S.B. Prusiner, D. Groth, A. Serban, et al., *Proc. Natl. Acad. Sci. USA* 90 (1993) 10608–10612.
- [41] B. Caughey, R.E. Race, D. Ernst, M.J. Buchmeier, B. Chesebro, *J. Virol.* 63 (1989) 175–181.
- [42] D.R. Borchelt, M. Scott, A. Taraboulos, N. Stahl, S.B. Prusiner, *J. Cell Biol.* 110 (1990) 743–752.
- [43] D.G. Donne, J.H. Viles, D. Groth, et al., *Proc. Natl. Acad. Sci. USA* 94 (1997) 13452–13457.
- [44] R. Riek, S. Hornemann, G. Wider, M. Billeter, R. Glockshuber, K. Wuthrich, *Nature* 382 (1996) 180–182.
- [45] R. Riek, S. Hornemann, G. Wider, R. Glockshuber, K. Wuthrich, *FEBS Lett.* 413 (1997) 282–288.
- [46] D. Riesner, K. Kellings, K. Post, et al., *J. Virol.* 70 (1996) 1714–1722.
- [47] J. Hofrichter, P.D. Ross, W.A. Eaton, *Proc. Natl. Acad. Sci. USA* 71 (1974) 4864–4868.
- [48] M.P. McKinley, D.C. Bolton, S.B. Prusiner, *Cell* 35 (1983) 57–62.
- [49] R.K. Meyer, M.P. McKinley, K.A. Bowman, M.B. Braunfeld, R.A. Barry, S.B. Prusiner, *Proc. Natl. Acad. Sci. USA* 83 (1986) 2310–2314.
- [50] D. Westaway, G. Telling, S. Priola, *Proc. Natl. Acad. Sci. USA* 95 (1998) 11030–11031.
- [51] S.J. Dearmond, M.P. McKinley, R.A. Barry, M.B. Braunfeld, J.R. McColloch, S.B. Prusiner, *Cell* 41 (1985) 221–235.
- [52] R.A. Somerville, L.A. Ritchie, P.H. Gibson, *J. Gen. Virol.* 70 (1989) 25–35.
- [53] M.M. Robinson, W.P. Cheevers, D. Burger, J.R. Gorham, *J. Infect. Dis.* 161 (1990) 783–786.
- [54] S.J. Dearmond, W.C. Mobley, D.L. Demott, R.A. Barry, J.H. Beckstead, S.B. Prusiner, *Neurology* 37 (1987) 1271–1280.
- [55] M. Guentchev, M.H. Groschup, R. Kordek, P.P. Liberski, H. Budka, *Brain Pathol.* 8 (1998) 615–623.
- [56] J.R. Scott, H. Fraser, *Brain Res.* 504 (1989) 301–305.
- [57] R.J.H. Payne, D.C. Krakauer, *Proc. Royal Society of London*, 1998, Vol. 265, N. 1412, p. 2341–2346.
- [58] A.J. Raeber, R.E. Race, S. Brandner, et al., *EMBO J.* 16 (1997) 6057–6065.
- [59] Y.O. Chernoff, S.L. Lindquist, B. Ono, S.G. Ingevechto-mov, S.W. Liebman, *Science* 268 (1995) 880–884.
- [60] S.V. Paushkin, V.V. Kushnirov, V.N. Smirnov, M.D. Ter-Avanesyan, *EMBO J.* 15 (1996) 3127–3134.
- [61] V.V. Kushnirov, M.D. Ter-Avanesyan, *Cell* 94 (1998) 13–16.
- [62] S.K. DebBurman, G.J. Raymond, B. Caughey, S. Lindquist, *Proc. Natl. Acad. Sci. USA* 94 (1997) 13938–13943.